Long-Range Predictability in the Tropics. Part II: 30–60-Day Variability

THOMAS REICHLER* AND JOHN O. ROADS

Scripps Institution of Oceanography, University of California, San Diego, La Jolla, California

(Manuscript received 10 March 2003, in final form 24 June 2004)

ABSTRACT

It is suggested that the slow evolution of the tropical Madden–Julian oscillation (MJO) has the potential to improve the predictability of tropical and extratropical circulation systems at lead times beyond 2 weeks. In practice, however, the MJO phenomenon is extremely difficult to predict because of the lack of good observations, problems with ocean forecasts, and well-known model deficiencies. In this study, the potential skill in forecasting tropical intraseasonal variability is investigated by eliminating all those errors. This is accomplished by conducting five ensemble predictability experiments with a complex general circulation model and by verifying them under the perfect model assumption. The experiments are forced with different combinations of initial and boundary conditions to explore their sensitivity to uncertainties in those conditions.

When "perfect" initial and boundary conditions are provided, the model produces a realistic climatology and variability as compared to reanalysis, although the spectral peak of the simulated MJO is too broad. The effect of initial conditions is noticeable out to about 40 days. The quality of the boundary conditions is crucial at all lead times. The small but positive correlations at very long lead times are related to intraseasonal variability of tropical sea surface temperatures (SSTs). When model, initial, and boundary conditions are all perfect, the useful forecast skill of intraseasonal variability is about 4 weeks. Predictability is insensitive to the El Niño–Southern Oscillation (ENSO) phenomenon, but it is enhanced during years when the intraseasonal oscillation is more active.

The results provide evidence that the MJO must be understood as a coupled system. As a consequence, it is concluded that further progress in the long-range predictability effort may require the use of fully interactive ocean models.

1. Introduction

The intraseasonal or Madden–Julian oscillation (MJO) is the dominant mode of low-frequency variability in the tropical troposphere (e.g., Madden and Julian 1994). It consists of large-scale perturbations in the tropical wind field that tend to propagate eastward at typical periodicities between 30 and 60 days. The slow evolution of the MJO relative to "weather" and its importance for the tropical diabatic heating field suggest that a realistic simulation of the oscillation may improve long-range forecasts (between 2 weeks and one season). Winkler et al. (2001) demonstrated with a linear model that the consideration of tropical heating, which is associated with the MJO and other effects, can produce predictability as far as 7 weeks ahead. Another key aspect of the MJO is that it also impacts the variability and predictability of the extratropical circulation (Ferranti et al. 1990; Higgins and Mo 1997; Jones et al. 2004).

Although better simulations of the MJO may have the potential to improve long-range forecasts, the practical realization of this effect is hampered by several factors. First of all, the MJO is a very sporadic phenomenon and is therefore difficult to predict. Furthermore, cumulus convection, which seems to be a key aspect of the MJO, is only crudely represented in current models. The exact physical mechanisms of the MJO are also not well understood. It is, for example, not exactly clear what the role of air–sea interaction is for the simulation of the MJO. The consequence is that current models have notorious problems in simulating an adequate MJO (e.g., Slingo et al. 1996). Additional complications arise from large observational errors that are contained in tropical analysis. Those errors, which are introduced into the forecast through the initial conditions (ICs), are related to the sparse observational network and the lack of direct observations of divergence and diabatic heating, which are important for the simulation of the MJO (Hendon et al. 2000).

* Current affiliation: Department of Meteorology, University of Utah, Salt Lake City, Utah.

Corresponding author address: Dr. John O. Roads, Scripps Institution of Oceanography, University of California, San Diego, 9500 Gilman Dr., La Jolla, CA 92093-0224.
E-mail: jroads@ucsd.edu

Relatively few studies have examined the skill in forecasting tropical intraseasonal variability with dynamical models. Chen and Alpert (1990), for example, used the medium-range forecast (MRF) model and found that the useful forecast limit of filtered upper-level velocity potential is about 8 days. Very similar results were found in studies by Lau and Chang (1992), Boer (1995), and Jones et al. (2000). This short predictability range does not really offer much hope for improving long-range predictability, and it is also surprising when considering the intuitive notion that predictability for a given process should be approximately proportional to its lifetime (Van den Dool and Saha 1990).

The previous predictability studies had three important things in common: First, forecasts were verified against observations, so that well-known model deficiencies led to a dramatic decrease in predictability. Second, the forecasts were initialized from operational analyses, which are known to be particularly problematic in the Tropics. Third, predictability was understood as a pure initial condition problem, and the possible role of air–sea interaction for the MJO was largely neglected. For example, the Dynamical Extended Range Forecasts (DERF) experiments from the National Centers for Environmental Predictions (NCEP) used sea surface temperatures (SSTs), which were damped to climatology from observed initial states (Schemm et al. 1996). There is, however, growing evidence that in addition to atmospheric internal dynamics, thermodynamic processes from the ocean interacting with the atmosphere are important in sustaining the MJO (e.g., Flatau et al. 1997; Waliser et al. 1999b). Very recently, Schubert and Wu (2001) and Wu et al. (2002) found that prescribing observed weekly SSTs as boundary conditions (BCs) to atmospheric general circulation models (AGCMs) led to significant MJO-like responses. The modeled SST influence seemed to be strongest over the Indian and western Pacific Oceans, where the MJO accounted in some cases for more than 25% of the total intraseasonal variance.

Our goal in the present paper was to understand the potential predictability properties of tropical intraseasonal variability in a perfect predictability experiment where the physical representation (model), initial, and boundary conditions are known. This research was also aimed at understanding how sensitive forecasts of tropical intraseasonal variability are to uncertainties in initial and boundary conditions. To this end, we conducted five AGCM predictability experiments using different combinations of initial and boundary conditions.

In a companion paper (Reichler and Roads 2005, hereafter referred to as RR), we investigate the predictability of monthly means in the Tropics. The main difference between the two studies is variability on interannual time scales, which is contained in monthly means, but which has been eliminated in this study. For monthly means, boundary conditions are the main contributor to predictability, but we also found substantial sensitivity to initial conditions. For forecasts of intraseasonal variability, initial conditions are of course crucial, but how sensitive is the MJO to uncertainties in the definition of boundary conditions? This question is of practical importance since operational forecasts use SST boundary conditions that may contain large errors, either because simple methods like climatological or persisted SSTs are used or because of the limitations of the used ocean model.

Several idealized assumptions are made in this study. First, to eliminate model induced errors, we use the so-called perfect model assumption (Buizza 1997; Anderson et al. 1999) and verify one forecast against another forecast with the same model. Second, we make hindcast experiments with prescribed ocean boundary conditions, which assumes that the future evolution of the ocean is known a priori. Third, we measure predictability from a particular model, which does not behave exactly like the real physical system. For example, the model may over- or underestimate the sensitivity of the atmosphere to boundary forcing. In general, the potential perfect model predictability, which we derive here, is likely to be higher than practical predictability, where observational data are used to initialize and verify the model and where predicted ocean data are used as to force the model. It also should be mentioned here that the use of prescribed ocean boundary conditions is somewhat problematic given the growing body of evidence that the MJO in the real atmosphere must be understood as a coupled process, whereby the interaction of the atmosphere with the ocean plays an important role.

This paper is structured as follows: Methodological aspects are discussed in section 2. General features of the simulated intraseasonal variability are described in section 3. In section 4, the skill in forecasting intraseasonal variability is examined for the different experiments. In section 5, the impact of initial and boundary conditions is described using a phase space representation. In section 6, the forced component of intraseasonal variability and its relationship to the SSTs is examined in more detail. Summary and conclusions are presented in section 7.

2. Methodology

Most of the methodological aspects of this study are the same as in RR, so only a brief overview is given here.

The AGCM of this study was the NCEP seasonal forecasting model (SFM) with T42 horizontal resolution and 29 vertical sigma layers. The cumulus convection parameterization of this model, which is a particularly crucial element for the simulation of tropical intraseasonal variability, was the "relaxed Arakawa–

Schubert" (RAS) scheme (Moorthi and Suarez 1992). The model was used to conduct global simulations of 22 northern winter seasons (15 December–31 March) from 1979 to 2000. For each experiment and season, ensembles of 10–20 forecasts were produced. Simulations for each experiment, year, and season were forced with identically evolving boundary conditions but were started from slightly different initial conditions. The initial conditions were derived from long continuous base runs with the same model and were perturbed using the breeding technique (Toth and Kalnay 1993; Toth and Kalnay 1997).

Five experiments using different combinations of initial and boundary conditions were conducted. The experiments are designated by specific acronyms, which indicate the type of initial and boundary conditions. The control experiment ICBC was forced with observed weekly varying ocean boundary conditions. It was initialized from a base run, which was also forced with observed ocean boundary conditions. This is similar to using "observed" initial conditions under a real forecast situation. By verifying ICBC against itself we actually determined the upper limit of predictability, which would be achieved if the real atmosphere behaved exactly like the model and if initial and boundary conditions were almost perfectly known at the time of the forecast. Two more experiments were forced with the same boundary conditions as ICBC: experiment BC, which was started from randomly chosen "climatological" initial conditions, and experiment iBC, which was started from "adjusted" initial conditions (for details, see RR). The remaining two experiments were started from the same "perfect" initial conditions as ICBC, but experiment IC was forced with climatological, and ICP was forced with persisted ocean boundary conditions.

Before analyzing the model data, they were treated in the following way: The daily climatological mean annual cycle of the corresponding experiment was first removed. We refer to these anomalies as unfiltered data. Next, the data were filtered in time by applying a 30–60-day bandpass filter. The filtering was performed separately at each 107-day-long forecast time series, at each grid point, over all members, and over all years. The filtering was achieved by an iterative moving average procedure similar to that described by Waliser et al. (1999a). First, a 25-day moving average filter was applied four times to remove variability longer than 60 days. Each filtered time series became the input for the next pass. The smoothed time series was subtracted from the original data to remove variations of 60 days and longer. Then, a 9-day moving average filter was applied four times to remove variability of less than 30 days. The additional data at the beginning and end of the time series were generated by fitting at each pass of the moving average an autoregressive model of order 5 to the forecasts. However, since this procedure is problematic, we excluded in most of our analysis the first and last 12 days of the time series.

The predictability of intraseasonal variability was derived from the forecast skill of four variables: 200-hPa velocity potential (χ200) and 850-hPa zonal winds (U850), both of which represent very common measures of MJO activity, as well as 850-hPa temperatures (T850) and precipitation. Throughout most of this study, the Tropics are defined as the equatorial region between $\pm30°$ latitude. In some of our analysis, however, we restrict our attention to meridional averages between $\pm10°$ latitude, which corresponds roughly to the equatorial Rossby radius. This was done because the MJO is an equatorially trapped phenomenon and because the averaging reduces the dimensionality of the problem. The forecast skill was measured from temporal correlations as well as from spatial anomaly correlations over the tropical domain. The correlations were calculated between 10-member ensemble means of the experiment under consideration and individual realizations of the verifying control experiment ICBC. The average correlation over each of the 20 members of ICBC was taken as the final result. The averages were calculated using the Fisher z-transformation (see RR for more details on the calculation of the correlations).

3. Observed and simulated intraseasonal variability

In RR, we discussed the climatology and interannual variability of the SFM model in the Tropics. We found that key variables of the tropical circulation compare well with observations. Here, we assess the ability of the SFM model to simulate intraseasonal variability to provide a context for the subsequent results, which are based primarily on model data.

a. Spatial distribution

Figure 1 presents maps of the standard deviation of intraseasonally filtered data from the model (left) and from NCEP–National Center for Atmospheric Research (NCAR) reanalysis (right) for the four variables of this study. The model captures well the general patterns and the amplitudes of the observed variability. In particular the typical increased amount of intraseasonal activity over the Eastern Hemisphere is reproduced well by the model, as can be seen from χ200, U850, and the precipitation. The only difference is that the simulated variance tends to be somewhat larger than the observed one. Figure 1 (bottom) also shows the intraseasonal variability of the SSTs that was used to force the experiments of this study. Except for a narrow band over the equatorial cold tongue of the Pacific, the intraseasonal SST energy tends to be largest over the Indian Ocean. This corresponds well with the increased amount of atmospheric intraseasonal energy over this region.

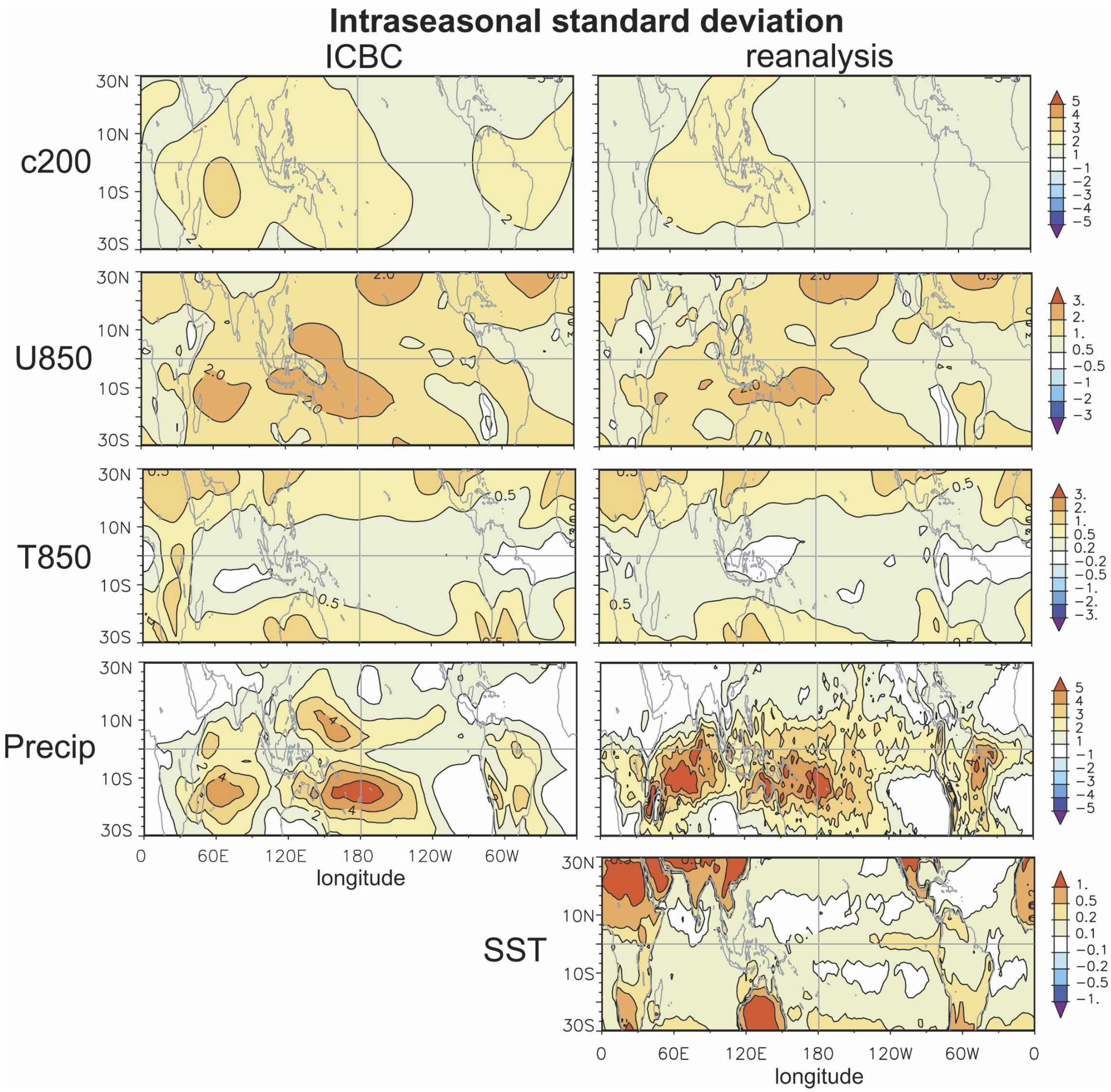

FIG. 1. The intraseasonal standard deviation of 30–60-day filtered velocity potential at 200 hPa (in 10^6 m^2 s^{-1}), zonal velocity at 850 hPa (in m s^{-1}), temperature at 850 hPa (in K), and precipitation rate (in mm day^{-1}). The fields were derived from (left) experiment ICBC and (right) the NCEP–NCAR reanalysis. The bottom right panel shows the variability of the SSTs that were used to force the model. Over land, it shows the variability of the skin temperatures from the NCEP–NCAR reanalysis (each in K).

b. Total and externally forced variability

Next we investigate how much of the total intraseasonal variability is caused by the external SST forcing. To this end, we separated the variance of $\chi 200$ into internal and external components as described in the appendix. The intra- and interensemble variances were calculated from intraseasonally filtered daily data for lead times of 41 days or greater to avoid influences from the initial conditions. Figure 2 shows the spatial distribution of the decomposition for data from simulations ICBC and IC and compares it with the total variance from NCEP–NCAR reanalysis. For easier presentation, only data along the equator were used. Again, the total variance (Fig. 2a) of simulation ICBC is somewhat larger but otherwise similar to the reanalysis in both magnitude and spatial distribution. Simulation IC, which was forced with climatological SSTs and therefore does not have a forced component, had, almost everywhere, a smaller amount of total variability than ICBC.

Figure 2 shows the ratio of external to total intrasea-

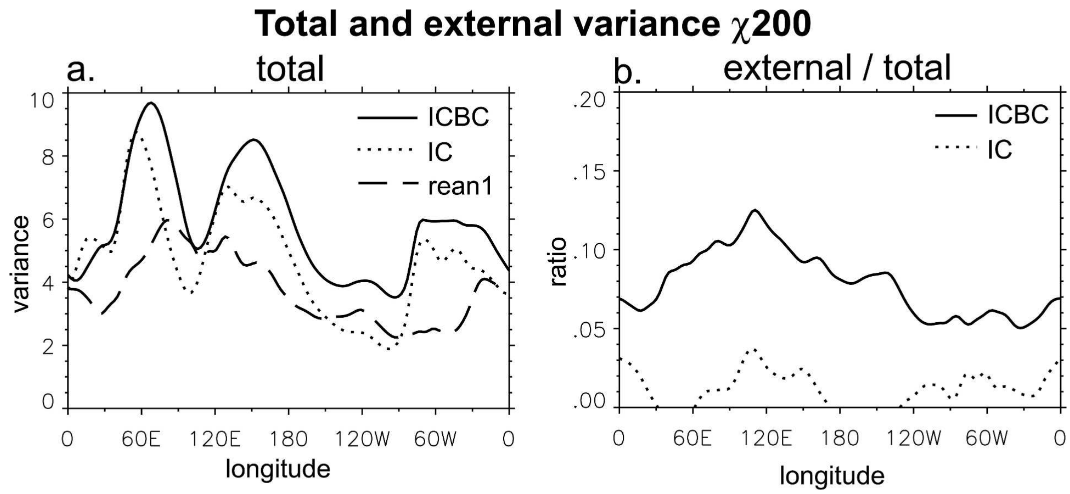

FIG. 2. (left) The total variance and (right) the ratio of external to total variance of filtered (30–60 days) 200-hPa velocity potential at the equator (±0°), as a function of longitude. The data were derived from experiment ICBC (continuous), experiment IC (dotted), and the NCEP–NCAR reanalysis (dashed). Units are 10^{12} m^4 s^{-2}.

sonal variability for the two simulations. As expected from the climatological boundary forcing, simulation IC had virtually no forced variability. Simulation ICBC, on the other hand, exhibited a ratio of external to total variance of about 0.1, with a maximum over the Indian Ocean region. This maximum coincides well with the region of maximum intraseasonal SST activity shown in Fig. 1. The ratio exhibited by simulation ICBC was similar to the values found in the study by Wu et al. (2002) from 10 different AGCMs over two full years. Overall, this demonstrates that SST forcing affects atmospheric intraseasonal variability but also that this effect is rather small.

c. *Wavenumber–frequency spectra*

We now describe the characteristics of the simulated intraseasonal variability in terms of wavenumber–frequency spectra of $\chi 200$ from NCEP–NCAR reanalysis and from experiments ICBC and IC. The spectra were calculated individually for each member and year, and averages were then taken for the final result. In the reanalysis (Fig. 3a), the eastward-propagating wavenumber 1 was the largest component. This wavenumber had a broad spectral peak centered on a 54-day period, which is traditionally attributed to the MJO phenomenon. The secondary maximum at zero frequency corresponds to the seasonal mean since interannual variability was not removed from the data.

The spectrum from experiment ICBC (Fig. 3b) exhibits more energy at zero frequencies than the reanalysis. This larger amount of interannual variability is probably related to different sensitivities to ENSO, which are probably due to the different cumulus convection parameterizations in the reanalysis model and in the model used for this study. More relevant for this study is that simulation ICBC also has a concentration of energy in the eastward-propagating wavenumber-1 component, which is typical for the intraseasonal oscillation. The main shortcoming of the model is that the energy is less concentrated in a single wavenumber in comparison to the reanalysis, and there are somewhat higher frequencies, both of which are typical problems for most AGCMs (e.g., Hayashi and Golder 1993; Kuma 1994; Slingo et al. 1996). The spectrum for simu-

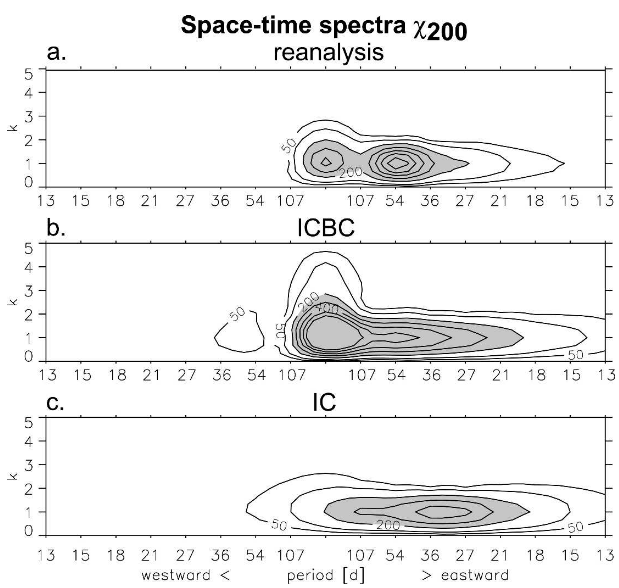

FIG. 3. Wavenumber–frequency spectra of unfiltered 200-hPa velocity potential from daily fields of the 1979–2000 period: from (a) the NCEP–NCAR reanalysis, (b) experiment ICBC, and (c) experiment IC. Units are 10^{12} m^4 s^{-2} day. Contour levels are 50, 100, 200, 300, 400, 500, and 600. Shading indicates values greater than 200.

lation IC is shown in Fig. 3c. Simulation IC exhibits less energy than ICBC at all frequencies, which must be a consequence of the forcing with climatological boundary conditions. Moreover, the spectral peak of IC is located at an even higher frequency than for ICBC, indicating that the intraseasonal oscillation of this model is sensitive to the kind of boundary forcing.

d. Composite MJO

Further characteristics of the intraseasonal variability in the reanalysis and model can be gathered from the time–longitude representation of composite events (Fig. 4). The composites were calculated by averaging over the 10 strongest events based on the anomalies at the base point at 150°E. The compositing was done for both filtered χ200 and U850. For χ200 (Fig. 4, top), both simulations show well-defined eastward-propagating signals that agree well with the reanalysis. The intraseasonal activity in the simulations tends to be spatially more localized than in the reanalysis. Again, one can see from the patterns that simulation IC has a shorter periodicity than ICBC. For U850 (Fig. 4, bottom), the eastward-propagating oscillations are present, but they are less coherent, in particular over the Pacific Ocean and for simulation IC.

Overall, these results demonstrate that the SFM is able to perform reasonable simulations of the intraseasonal oscillation when it is forced with observed SSTs. The model shows a clear eastward-propagating signal with realistic strength and periodicity. The main shortcoming is that the model is unable to simulate the dominance of the intraseasonal oscillation at periods of 50 days. There is too much power at higher frequencies, particularly when the model is forced with climatological SSTs.

4. Forecast skill of intraseasonal variability

a. Lead time evolution

In this section, we examine the temporal evolution of the perfect model forecast skill for the five experiments. As before, we used daily fields of intraseasonally filtered χ200, U850, T850, and precipitation. The forecast skill was measured from the spatial anomaly correlation over the tropical domain ($\pm$30°) between the ensemble mean of one experiment and individual members of the reference experiment ICBC. Figure 5 presents for each variable and experiment the evolution of the anomaly correlation (AC) from day 12 (27 December) out to day 94 (19 March). Each curve represents the average over 440 individual measurements, resulting from the 20 verification members from ICBC and from the 22 winter seasons (1979–2000).

The curves for simulation ICBC provide the upper limit of predictability with this model, because both the initial and the boundary conditions were perfect, except for small perturbations in the initial conditions. The curves for ICBC show the classical loss in predictability as the solutions for the individual ensemble members diverge with lead time. After 30–40 days or so, the de-

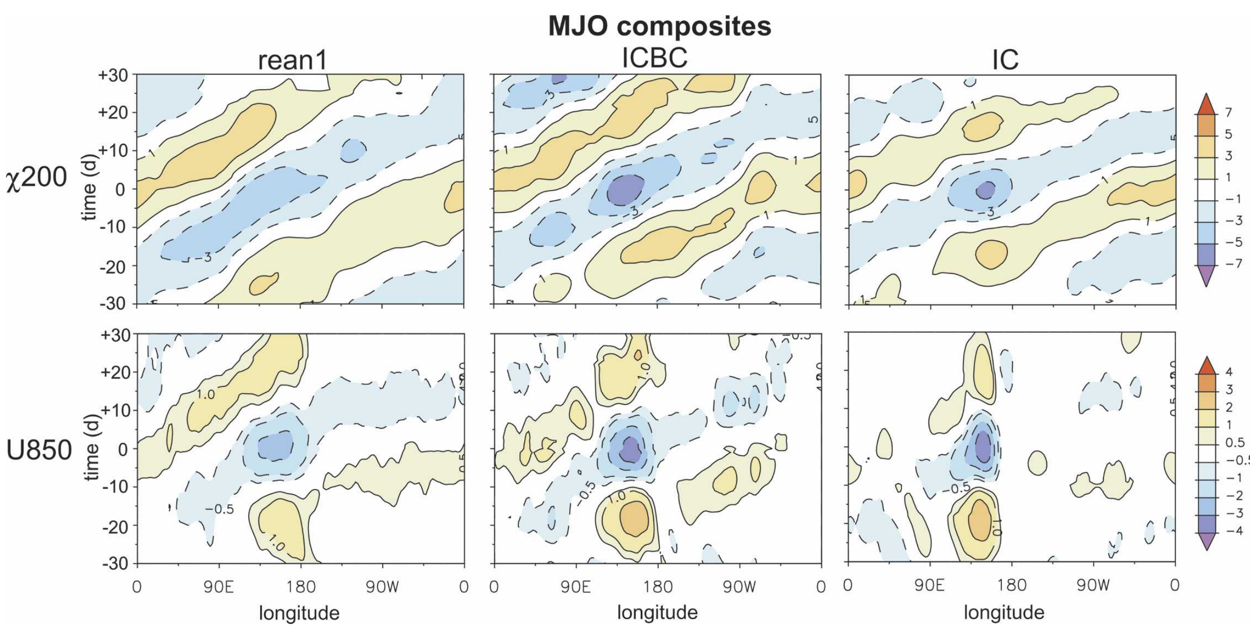

Fig. 4. Composite MJO events as a function of time and longitude of 30–60-day filtered (top) velocity potential at 200 hPa (in 10^6 $m^2 s^{-1}$) and (bottom) zonal wind at 850 hPa (in $m s^{-1}$) along the equator ($\pm$30°). The data were derived from (left) reanalysis and from one arbitrarily chosen member of experiments (middle) ICBC and (right) IC. The composites represent averages over the 10 time series with the strongest anomalies at 150°E.

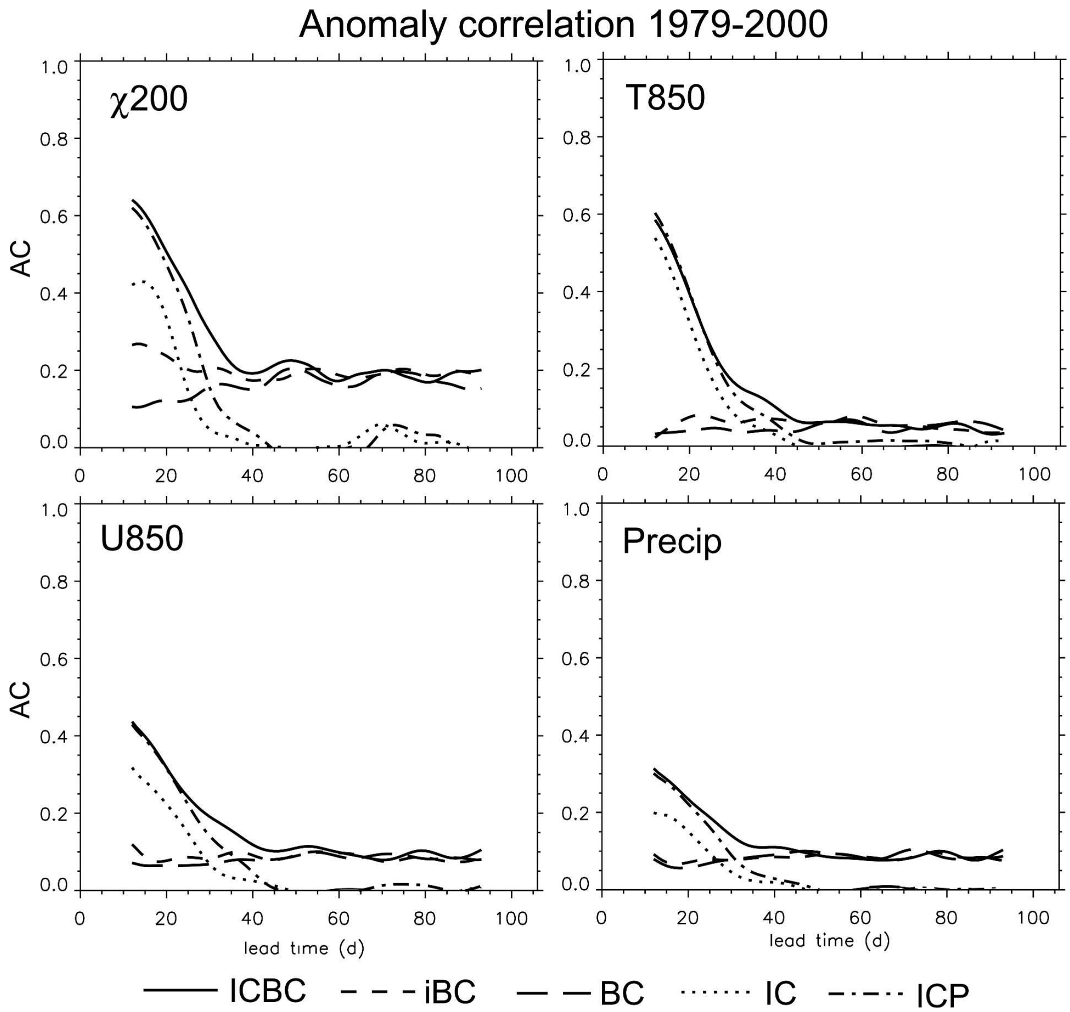

FIG. 5. The lead time evolution of the spatial AC over the Tropics (±30°) for four different filtered (30–60 days) model variables derived from the five experiments of this study. The results are averages over all 22 yr.

terministic predictability of ICBC was completely lost, and the correlations approached their asymptotic value. This small but nevertheless nonzero correlation at longer lead times must be due to the forced component of intraseasonal variability and the resulting nonzero signal-to-noise ratio. As we will show later, this is due to the small amount of variance in the MJO band, which is contained in the SST forcings.

The general shape of the curves for the different variables is very similar. The only major difference is the basic level of skill, which is highest for $\chi200$ and lowest for precipitation. This reflects the well-known differences in temporal and spatial variability for the different fields. If a correlation of 0.4 is taken as the minimum for useful skill, then the limit of predictability of intraseasonal variability is reached at about 4 weeks for $\chi200$, at about 3 weeks for U850 and T850, and practically never for precipitation.

Experiments IC and ICP were also started from perfect initial conditions, so that the correlations were also high at the beginning. However, the correlations drop off at a much faster rate than ICBC, presumably because of the lower quality of boundary conditions. For experiment ICP, which was forced with persisted SSTs, the range of useful predictability for $\chi200$ is about 1 week less than for ICBC. The correlations for experiment IC, which had to adjust to climatological boundary conditions, decayed even faster. Both experiments reached zero skill at about a 40-day lead time. This indicates how important the kind of boundary forcing is for the simulation of intraseasonal variability.

Experiment BC was initialized from climatological initial conditions, so that its correlations should be zero at zero lead time. From experiment iBC, one would expect a more or less constant skill in time since it was initialized from adjusted initial conditions. The results in Fig. 5 confirm that these assumptions are about right. At longer lead times, the correlations of iBC and BC approach the same asymptotic value as ICBC since all three simulations were forced with the same observed boundary conditions.

We were also interested in determining how sensitive our results were with respect to interannual SST variations in relation to ENSO. The demonstration of a connection between ENSO and the MJO has been controversial. Some studies suggested that the activity of the MJO was controlled by ENSO (e.g., Gutzler 1991; Fink and Speth 1997), while others found little evidence for such a link (e.g., Slingo et al. 1999; Hendon et al. 1999). We repeated the calculation of the ACs by excluding strong ENSO years from our calculations (not shown). The ACs for the weak-to-neutral ENSO years were very similar to those using all years, indicating that ENSO-related boundary forcing has little effect on the forecast skill of intraseasonal variability with our model.

b. Interannual variations and relationship to activity

We now examine a year by year breakdown of forecast skill for $\chi 200$ to show how important initial and boundary conditions were during individual years. As before, the skill was measured from the spatial anomaly correlations over the Tropics. We present for each year the AC averaged over a short (days 12–40) and a long (days 41–94) lead time interval. During the short lead time interval, the deterministic predictability from the initial conditions was high, and during the long lead time interval, the forced intraseasonal variability was dominating.

Figure 6 (top) presents the average ACs for the short lead time interval for simulations that were started from good initial conditions (ICBC, IC, and ICP). The bars on the very right (labeled ALL) show the average over all years. They confirm that on average, the forecast skill for experiment IC was much smaller than that for ICBC. However, it is surprising to see that during some years (e.g., 1988 and 1996), the correlations from IC were almost as good as those from ICBC. On the other hand, during other years (e.g., 1983, 1989, and 1993), simulation IC had much smaller skill than ICBC. This behavior suggests that the intraseasonal variability can sometimes be a very robust feature that is strongly determined by the initial conditions, while in other years this variability can be extremely sensitive to the additional uncertainties introduced by boundary forcing.

Figure 7 (top) shows the year-to-year variations in forecast skill during the long lead time interval (days 41–94). Only results for ICBC, iBC, and BC are presented, since those experiments were forced with perfect boundary conditions. At this long lead time, forecast skill results mostly from the forced intraseasonal response. This becomes clear from the bars on the very right, which show that the correlations of all three experiments averaged over all years are very similar.

The strong interannual variability in forecast skill exhibited by the experiments raises the question as to

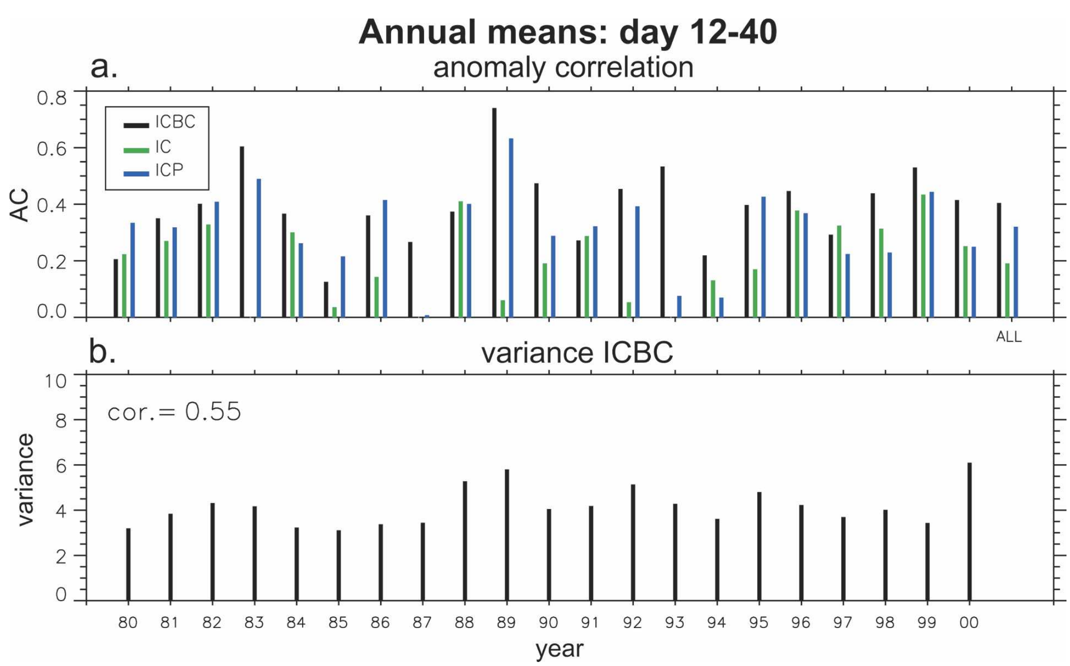

FIG. 6. The annual breakdown of (a) the ACs for experiments ICBC, IC, and ICP and (b) the spatiotemporal variance (in 10^{12} m^4 s^{-2}) of experiment ICBC. The calculations are based on filtered 200-hPa velocity potential over the tropical domain (±30°), and they represent temporal averages over the early lead time interval (days 12–40). The bars on the very right side (ALL) denote the mean correlations over all years.

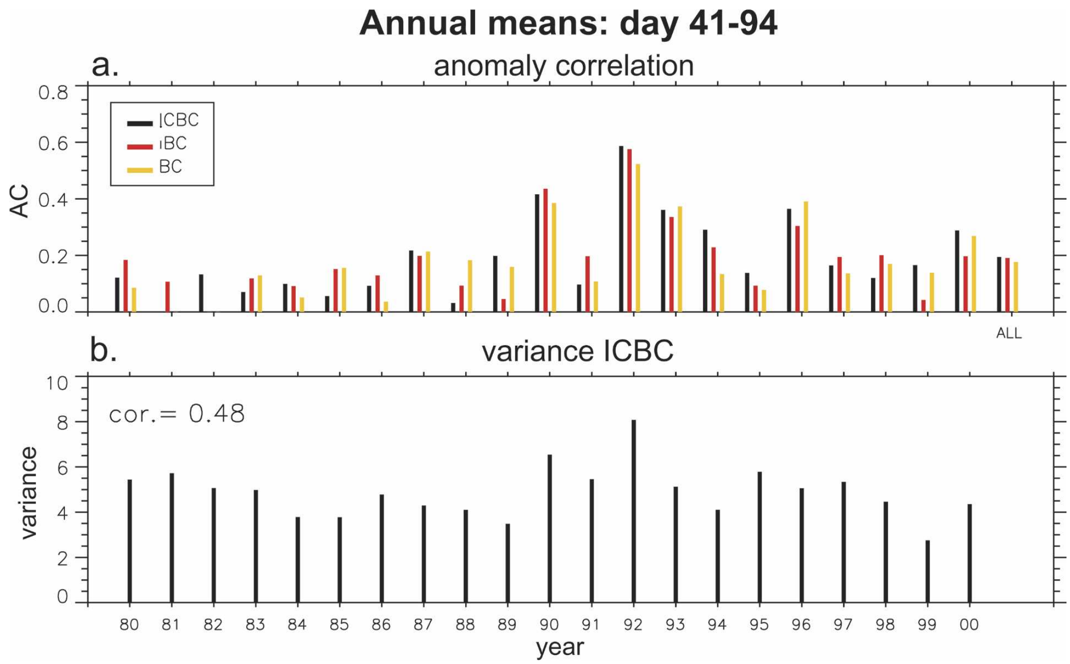

FIG. 7. Same as in Fig. 6, but for experiments ICBC, iBC, and BC, and for temporal averages over the late lead time interval (days 41–94).

whether there exists a relationship to the activity of the MJO during those years. The answer to this question has been very controversial in the past. Lau and Chang (1992), for example, found better skill; Boer (1995) found no impact; and Chen et al. (1993) found even lower skill when the MJO was more active. We now examine this relationship for simulation ICBC. The amount of intraseasonal activity during each year was measured from the spatiotemporal variance of bandpass-filtered χ200. This quantity is shown in the bottom panels of Figs. 6 and 7 for experiment ICBC and for the two lead time intervals. As one can see, the relationship between the year to year variations of forecast skill and amount of intraseasonal activity are modestly positive for our model. The correlations between skill and activity are 0.55 at the short lead time interval and 0.48 at the long lead time interval. Both correlations are statistically significant at the 95% error level.

c. Spatial distribution of forecast skill

Next, we discuss the spatial distribution of forecast skill. To this end, we calculated the temporal correlations (1979–2000) between a particular experiment and experiment ICBC for a specific location and lead time. These correlations were calculated at all grid points of the tropical domain to construct predictability maps. As before, we show temporal averages for a short (days 12–40) and a long (days 41–94) lead time interval. Figure 8 shows maps for the short lead time interval, during which the initial condition effect was strong. Only results from experiments ICBC, IC, and ICP are displayed since they were provided with good initial conditions. As expected, the various maps exhibit quite large differences in the basic levels of skill. However, a common feature of all experiments and variables is that their correlations are rather homogenously distributed in space. Experiment ICBC tends to have somewhat better forecast skill over the Eastern Hemisphere for χ200 and over the Western Hemisphere for T850 and precipitation. The other experiments do not exhibit such an east–west asymmetry. Predictability maps for the long lead time interval and for experiments ICBC, iBC, and BC are shown in Fig. 9. The maximum correlations tend to occur along the equator. For χ200, all experiments tended to have higher correlations over the Eastern than over the Western Hemisphere, indicating that this effect is related to the common boundary forcing. Note that a similar east–west asymmetry was found before in the analysis of variability (Figs. 1 and 2), with areas of higher correlations coinciding with areas of higher total and higher forced intraseasonal variability.

5. Phase space representation

We now demonstrate further the synchronizing effects of initial and boundary conditions on the intraseasonal variability. To this end, we examine the meridional average ($\pm 10°$) of χ200 along the equator, and we focus on the wavenumber-1 component of its complex Fourier expansion coefficients. The restriction to wavenumber 1 is meaningful since we have shown before

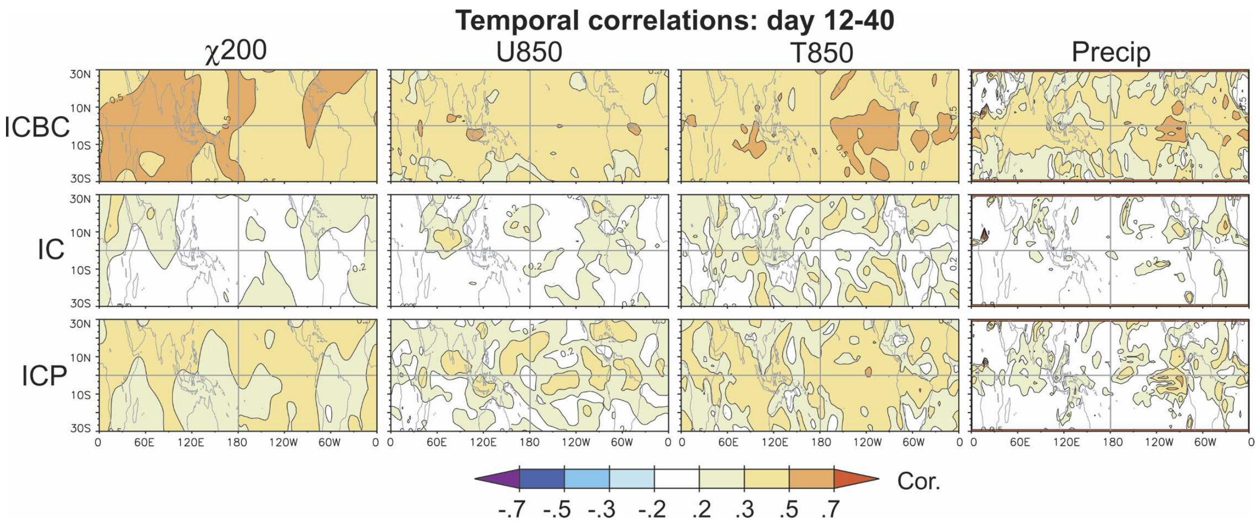

FIG. 8. The temporal correlations (1979–2000) for experiments ICBC, IC, and ICP of 30–60-day filtered data. Shown are averages for lead times between 12 and 40 days. All experiments were verified against ICBC.

that most of the intraseasonal energy of $\chi 200$ is contained in this spectral band. In fact, wavenumber 1 was often taken as the defining parameter for studies of the MJO (e.g., Lorenc 1984; Slingo and Madden 1991; Boer 1995). The advantage of this representation is that the full $\chi 200$ field is represented by just two variables, the phase and magnitude of its wavenumber-1 component. The phase represents the propagation of the intraseasonal oscillation, and the magnitude its strength or activity. The idea behind this approach is somewhat similar to the decomposition into two eigenmodes, which was more widely used in previous studies of the intraseasonal oscillation (e.g., Lorenc 1984; Chen and Alpert 1990; Ferranti et al. 1990; Jones et al. 2000).

The Fourier decomposition of intraseasonally filtered $\chi 200$ in the east–west direction along the equator is defined by

$$\chi_{200}(\lambda, t) = \sum_{m=-N}^{N} \mathbf{z}_m(t) e^{im\lambda}, \tag{1}$$

where z_m are complex Fourier expansion coefficients, and m is the wavenumber. The complex wavenumber-1 coefficient can be also written in polar coordinates,

$$z_1 = r \exp(\mathrm{i}\varphi).$$

The magnitude r represents the strength of the oscillation, and the phase φ represents the propagation.

From the previous discussion of interannual variability of forecast skill, we have shown that during some

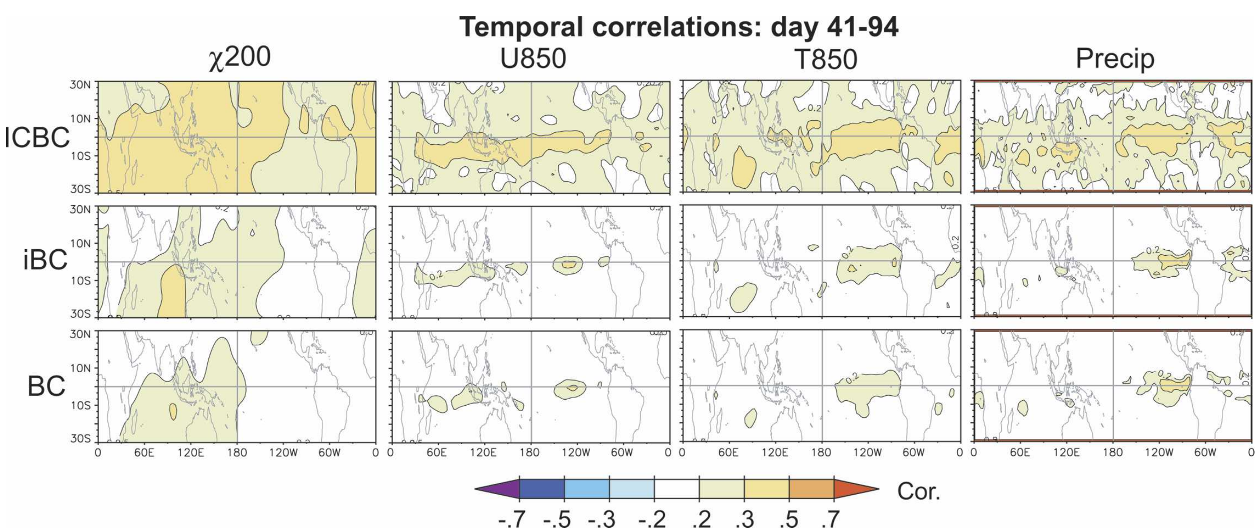

FIG. 9. Same as in Fig. 8, but for experiments ICBC, iBC, and BC and for lead times between days 41 and 94.

years the initial condition was important and that during other years the boundary condition effect was important. In the following, we use the phase space representation to examine the solutions of the various simulations during two particular years. Figure 10 shows the ensemble mean evolution of the wavenumber-1 Fourier coefficient of the filtered $\chi200$ in the complex plane. The magnitude r is represented by the distance to the origin, and the phase φ is represented by the angle from the positive x axis. Time is indicated by different colors. The magnitudes represent anomalies with respect to the 1979–2000 climatology.

Consider first the situation for 1992 (Fig. 10, top), a year during which the forced intraseasonal variability was important. The similarity of the trajectories gives an estimate for the similarity of the forecasts. At short lead times (0–20 days; red and orange colors), the trajectories of ICBC, IC, and ICP are similar because of the initial condition effect. On the other hand, experiment IC had regular intraseasonal oscillations, but the magnitude decreased gradually—either because of the decorrelation of individual member solutions or because of a decay of the amplitudes with increasing lag. The trajectory of ICP was quite distorted at longer lead times (green and blue colors), again indicating that the coherence between members was lost or that the amplitudes decayed. Experiment ICBC exhibited a regime shift at about day 30 (yellow color), and then continued with strong regular oscillations. After the shift, the trajectories of iBC and BC were very similar in phase as well as in magnitude to ICBC. This synchronous behavior must be due to the common forced variability component of all three experiments.

The bottom graphs of Fig. 10 represent the evolution of intraseasonally varying $\chi200$ during the year 1996. From Figs. 6 and 7, one can see that during this year the initial condition as well as the boundary-forced forecast skill (both with about 0.5 correlation) was modestly high. At short leads (red colors), the trajectories of ICBC, IC, and ICP agreed quite well. At longer leads, IC continued to oscillate quite regularly and performed a total of about 3.5 oscillations. Again, the trajectory of simulation ICBC exhibited a discontinuity at about day 20 (yellow color), and at longer leads (greenish and bluish colors), the trajectories of ICBC, iBC, and BC were reasonably similar.

6. Forced intraseasonal variability

It was shown before that SST forcing influences the atmosphere on intraseasonal time scales and that it produces a forecast skill of about 0.2 correlation at long lead times. The strength of this effect was highly variable from year to year, and it was particularly noticeable during the years 1990, 1992, 1996, and 2000. In this section, we further investigate the relationship between SST forcing, intraseasonal variability, and long-lead forecast skill.

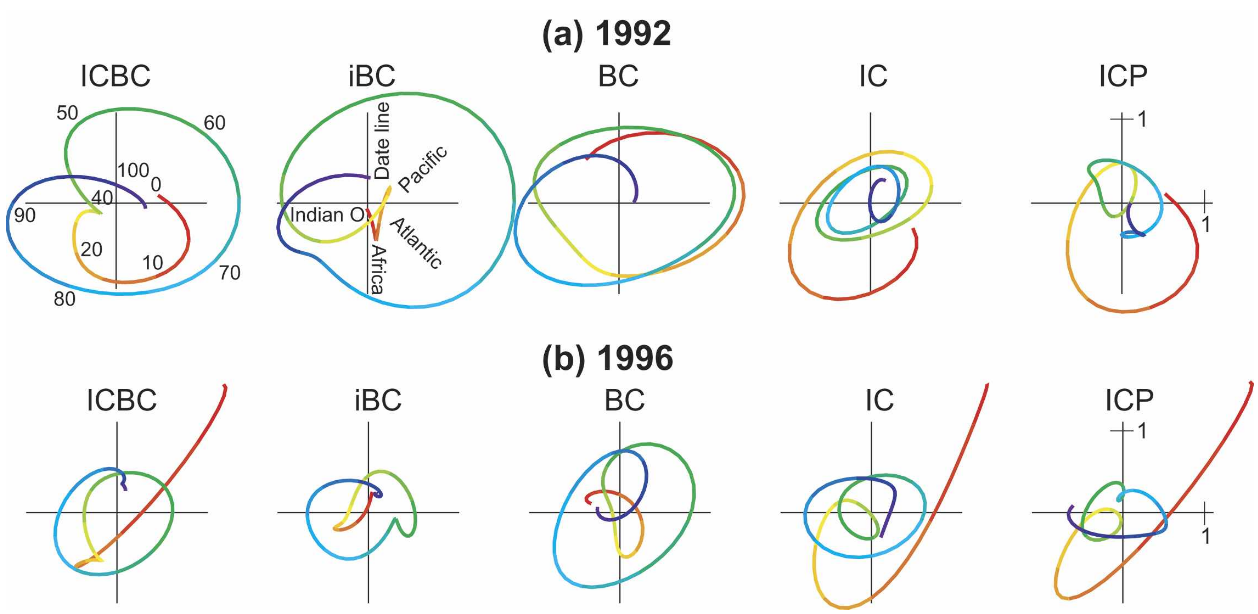

FIG. 10. The trajectory of the MJO in phase space for the different experiments during northern winter (a) 1992 and (b) 1996. Shown is the evolution of the complex wavenumber-1 coefficient of the 30–60-day filtered 200-hPa velocity potential along the equator (±10°). The distance from the center denotes the magnitude in 10^6 m^2 s^{-1} (see ICP). The angle from the positive x axis represents the phase. Time is shown in colors and by numbers (for ICBC 1992). The colors change every 5 days, starting with red (days 0–4) and ending with purple (days 105–107). The indicated geographical locations mark the approximate center of maximum convection for a given phase angle.

a. Tropical SST variability

We first show the spectral energy distribution of the SSTs that were used to force the experiments of this study. The goal is to find out whether there exist any links between SST variability and forecast skill. Figure 11 shows for each simulation year the amount of SST energy that is contained in the intraseasonal frequency band (54 days). Before the spectra were computed, the annual mean as well as the annual and semiannual seasonal cycle was removed from the SST data. In space, the spectra were calculated along the equator for all latitude bands between 10°N and 10°S, and the final result was averaged over those latitudes. Figure 11 shows intraseasonal energy in the SST data that varies from year to year. From previous studies, it is known that tropical SSTs have an intraseasonal peak (Krishnamurti et al. 1988), which can amount to local SST variations of 1.0°C and more (Weller and Anderson 1996). This peak is coherent with observed changes in surface heat fluxes and SSTs that occur during the passage of an MJO (e.g., Zhang 1996; Flatau et al. 1997; Maloney and Kiehl 2002).

The SSTs exhibit a clear energy maximum during the year 1992, and, incidentally, during the same year, the long-lead forecast skill and the amount of atmospheric intraseasonal variability were large too. This can be seen from a comparison with Fig. 7. The correlation between the intraseasonal SST energy (Fig. 11) and the forecast skill for ICBC (top of Fig. 7) is 0.58. This is relatively high, in particular when considering that such a relationship is not necessarily linear and that other factors beside SST forcing determine the correlations as well. We think that that SST patterns with a similar spatiotemporal structure as the intraseasonal oscillation are particularly effective in forcing atmospheric intraseasonal variability, much in the sense of a resonant forcing of a dynamical system. This can explain the relatively good relationship between the amount of SST variability, atmospheric variability, and long-lead forecast skill in the intraseasonal band.

b. Case study

Let us examine the situation for 1992 in more detail. Figure 12 presents a comparison of unfiltered tropical SST anomalies (shading) and associated filtered $\chi 200$ (thick contours) from reanalysis (Fig. 12a) and simulation ICBC (Fig. 12b). The SSTs are identical in both panels and represent latitudinal averages from 10°N to 10°S. They exhibit the typical signature of an ENSO warm event, with warmer waters over the Pacific and colder waters over the warm pool region. As expected, there was strong intraseasonal variability on top of this mean pattern.

The overlaid $\chi 200$ for the reanalysis (Fig. 12a) reveals a good relationship between the intraseasonal activities of the ocean and the atmosphere: the ocean was warmer before the period of active convection (negative $\chi 200$) and cooler after it. The patterns of $\chi 200$ for simulation ICBC (Fig. 12b) also show a distinctive intraseasonal activity, which seems to be shifted by about one-quarter cycle toward earlier times with respect to the reanalysis. This leads to a more direct relationship between ocean and atmosphere, in the sense that anomalous rising motions tend to coincide directly with warm or neutral SST anomalies, and sinking motions coincide with cold SST anomalies. This suggests that SST forcing with proper frequencies is able to phase lock the simulated intraseasonal oscillation into its own cycle.

The intraseasonal SST variations over the warm pool region amount only to 0.6°C or so. It is curious that such small temperature variations control the intraseasonal activity in the model. To explain this behavior, it is important to understand that the atmospheric response to tropical SSTs is strongly nonlinear. Observations show that SSTs above 26–27°C are required for large-scale deep convection to occur and that little convective activity takes place over SSTs colder than that (e.g., Graham and Barnett 1987). Since the mean SSTs over the Indian Ocean during January were close to the 27°C threshold (not shown), even small SST anomalies

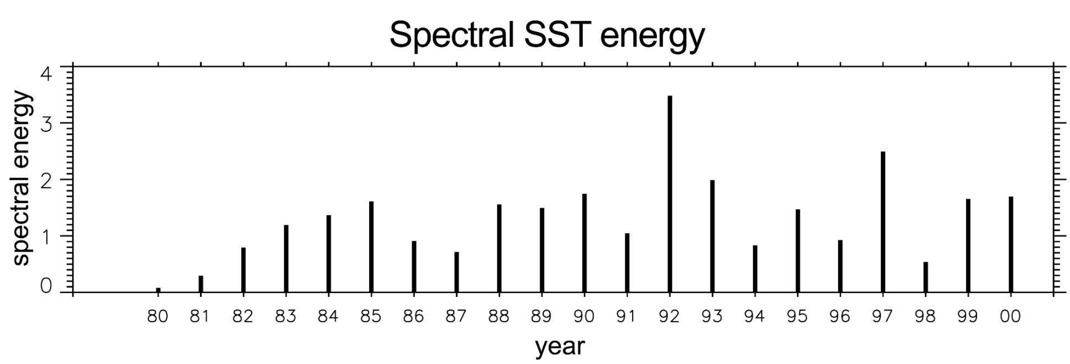

FIG. 11. The spectral energy of the SSTs (in K^2 day) that were used to force the experiments of this study. The SST data were taken from the equatorial strip (±10°). They were spectrally filtered in space and time to consider only energies at periods of 54 days and eastward-traveling wavenumbers from 0 to 3.

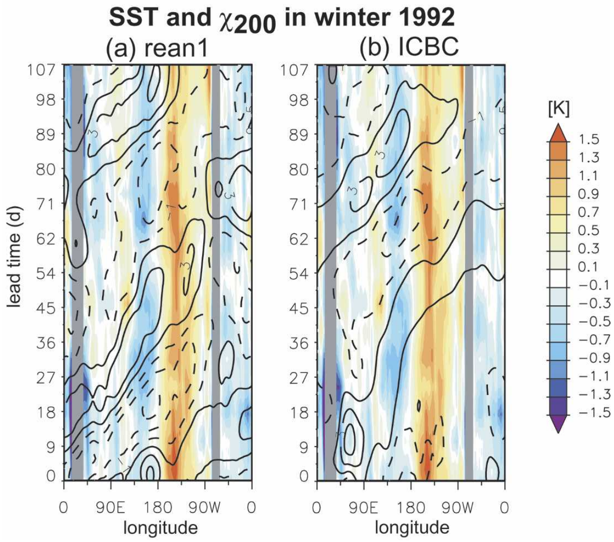

FIG. 12. The temporal evolution of the unfiltered SST anomalies (in K) along the equator (±10°) during the year 1992. The black contour lines show the 30–60-day filtered 200-hPa velocity potential for the corresponding time and location from (a) the NCEP–NCAR reanalysis and (b) experiment ICBC.

may have been very effective in controlling the convective activity.

c. SST–MJO relationship

We now establish a more general relationship between SST forcing and intraseasonal activity by using data from many events. Figure 13 shows composites of strong MJO events (thick contours) for simulation ICBC (top) and for reanalysis (bottom). Again, the composites were formed by selecting the *n* strongest MJO events from the intraseasonally filtered $\chi200$ over a specific base point. Taking into account the different ensemble sizes, *n* was 20 for the reanalysis and 200 for ICBC. Two base points were selected to capture different stages of the oscillation: one over the Indian Ocean (90°E), and one over the warm pool (150°E). All panels show strong intraseasonal SST variability, indicating again that intraseasonal SST variability was connected to a similar variability in the atmosphere. In the model (top), convection was enhanced (suppressed) by warm (cold) SST anomalies almost directly underneath. The associated SSTs for the reanalysis (bottom) were more noisy because of the smaller sample size. In this case, the regions of warmest SST anomalies tended to lead the convective anomalies by several days.

To better quantify the relationship between atmospheric and oceanic intraseasonal activity, we calculated cross correlations between the composite events and associated SST anomalies for different phase lags (Fig. 14). Temporal correlations were computed between the filtered $\chi200$ time series at a fixed grid point and the SST anomaly time series at different locations to the east or west of this point. Results from all grid points along the equator were averaged.

For the reanalysis (Fig. 14, continuous lines), the intraseasonal oscillation had the strongest negative correlations with SSTs at a phase lag of about 60° to the east or about 7 days. The two different base points led to very similar results. The correlations are negative since cool (negative) SST anomalies tend to suppress convection, which leads to positive $\chi200$ anomalies (upper-level convergence). The 60° phase shift agrees well with the general picture seen before: SSTs are higher before the period of active convection and lower after it. This is also in line with observational findings. For example, Flatau et al. (1997) showed that to the east of the convective region, increased shortwave radiation fluxes increased the SSTs, whereas in the vicinity and to the west of this region, cloud shielding and strong air–sea heat fluxes cooled the SSTs.

For simulation ICBC (Fig. 14, dashed lines), maximum negative correlations occur for SST anomalies at a phase lag of only about 10°E. This much smaller eastward shift reflects the different MJO–SST relationship between model and nature. In nature, intraseasonal SST variations are mostly caused by the atmosphere as described above. In our model, however, prescribed SSTs force the atmosphere above, so that the simulated intraseasonal oscillation tended to be almost in phase with the SST. This is in line with results by Wu et al. (2002), who found that simulated and observed $\chi200$ anomalies tend to be in quadrature with the simulations leading the observed anomalies by about 10 days.

7. Summary and conclusions

This study investigated the predictability of the tropical intraseasonal oscillation and its sensitivity to initial conditions and boundary forcing. Five types of AGCM experiments were conducted with the NCEP SFM, each with different combinations of initial and boundary conditions. The experiments simulated the state of the northern winter atmosphere over the 22-yr-long period from 1979 to 2000 with 10–20 ensemble members.

When the model was forced with observed weekly SSTs, it exhibited realistic intraseasonal variability. About 10% of it was accounted for by the thermodynamic forcing from the ocean. The model simulated the typical features of the MJO, but the spectral peak of the oscillation was too broad. When forced with climatological SSTs, this peak shifted toward higher frequencies, indicating that the simulation of the oscillation was sensitive to boundary forcing.

A predictability estimate of intraseasonal variability was derived from the perfect model forecast skill of four representative variables. The effects of initial conditions on the simulation of the intraseasonal variability lasted for about 40 days. With "perfect" initial and boundary conditions, the useful forecast range for $\chi200$

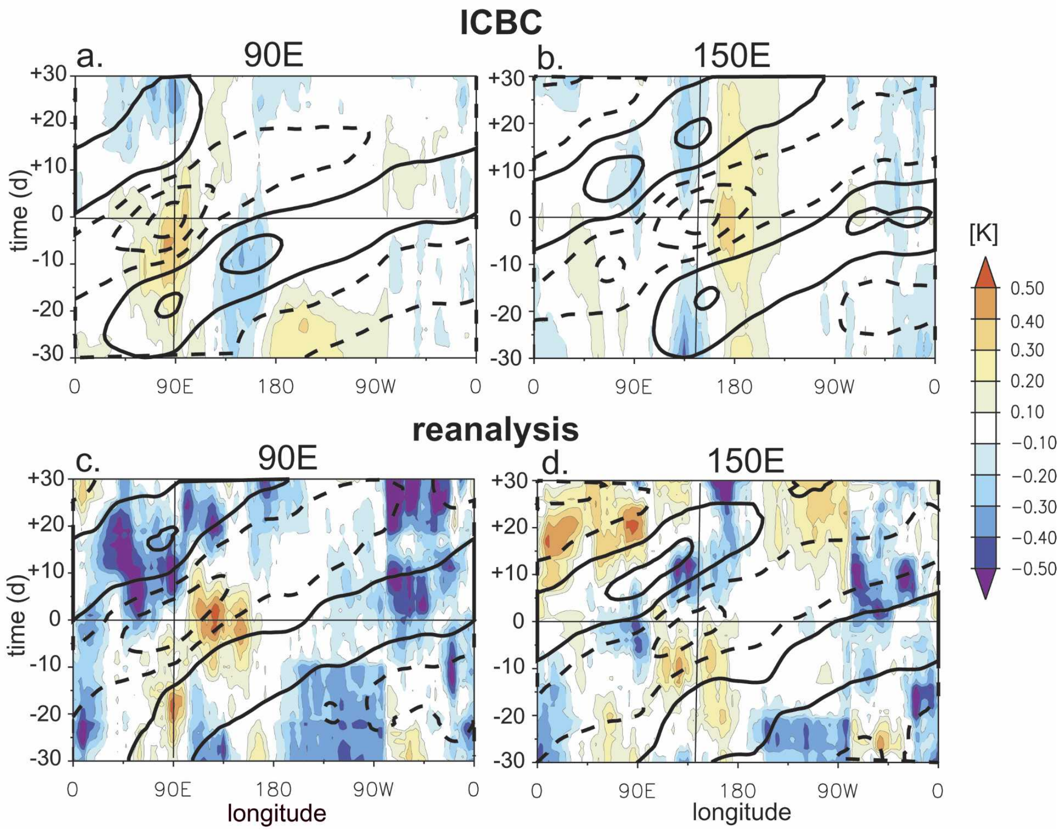

FIG. 13. Composite 200-hPa velocity potential (thick contours) and the associated SST anomalies (shading) along the equator (±10°) for (top) simulation ICBC and (bottom) reanalysis. Shown are composites of the 200 (ICBC) or 10 (reanalysis) strongest MJO events, as given by the strength of negative anomalies of 30–60-day filtered χ200 at the base point [(left) 90° and (right) 150°E]. The contour lines are from –6 to 6 × 10^6 m^2 s^{-1} in intervals of 2. Negative values are dashed. The SST anomalies were standardized by their local interannual standard deviation and are unitless.

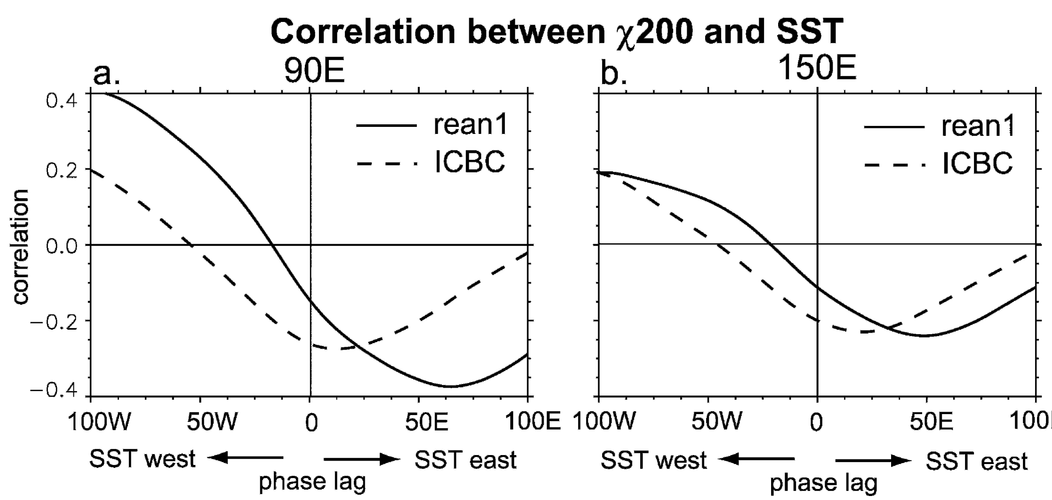

FIG. 14. The temporal correlation between the composite χ200 and SST events shown in Fig. 13 for base points at (a) 90° and (b) 150°E. The ordinate denotes temporal correlation, and abscissa denotes west- or eastward shift of SSTs in degrees longitude.

averaged out to 4 weeks. A recent study by Waliser et al. (2003) came to a very similar estimate of the potential predictability limit of the MJO using a different model and verification strategy. The 4-week range is much longer than the 8-day limit found from previous studies for the same variable. The main reason for this difference is our perfect model setting, where we completely eliminated model errors, ocean forecast errors, and observational errors in the initial conditions. Given the importance of tropical variability for global weather and climate, our results suggest that current long-range forecasting systems could be improved if the MJO could be represented better in current models.

The quality of boundary conditions was crucial for the simulation of intraseasonal variability. When using persisted instead of observed SSTs, the range of useful predictability was reduced to about 3 weeks, and with climatological SSTs, it was less than 10 days. We found that the predictability of intraseasonal variability was higher when the oscillation was more active, but we found no evidence for an influence of interannual SST variability in relation to ENSO. Even at very long lead times, the forcing with observed boundary conditions led to some forecast skill, which was related to the externally forced variability. Boundary forcing with a similar spatiotemporal structure as the MJO was particularly effective in influencing atmospheric intraseasonal variability: during years when the SST energy in the intraseasonal band was high, the forced intraseasonal response of the atmosphere was high and so was the forecast skill.

In a case study, we showed that strong intraseasonal variability in the tropical SST field phase locked the atmosphere into its own cycle. A more general relationship between atmospheric and oceanic intraseasonal variability was derived from examining many strong MJO events. When prescribed SST anomalies forced the intraseasonal variability, the atmosphere and the ocean tended to be in phase, with enhanced convection almost directly above positive SST anomalies. In nature, on the other hand, intraseasonal SST anomalies are mostly caused by the atmosphere. The consequence is a phase lag between both, in the sense that SSTs are higher before the period of active convection and lower after it. These different relationships point to a dilemma: The forced predictability, which was found in this study from prescribing weekly SSTs, does not imply the same predictability under real conditions. The problem is that SSTs themselves are to a large extent the product of the unknown atmospheric forcing. Nevertheless, the sensitivity of the MJO to prescribed boundary conditions may still imply real predictability, for example, through preexisting persistent SST anomalies.

Overall, this study suggests that practical forecast skill of tropical intraseasonal variability could be improved if the MJO modeling problem could be solved and if more realistic initial and boundary conditions could be obtained. Our results provided indirect evidence for the coupled nature of the MJO, which is inconsistent with the use of prescribed low-frequency ocean boundary conditions. Further progress in the long-range predictability effort may therefore be achieved with the use of fully coupled models.

Acknowledgments. Funding for this research was provided by a cooperative agreement with NOAA (NA77RJ0435 and NA17R1231) and NASA Grant NAG8-175. The views expressed herein are those of the authors and do not reflect the views of NOAA and NASA. We thank the Maui High Performance Computing Center and the San Diego Supercomputing Center for providing computing time. We thank M. Kanamitsu for many insightful discussions and for his help with the model. We appreciated the comments of three anonymous reviewers, which helped to improve this paper. This work is part of the Ph.D. thesis of T. Reichler.

APPENDIX

Total and External Variance

In some of our analysis, we decomposed the total variability of a variable into externally and internally generated components, or simply into signal and noise. Using simulations with many ensemble members, Rowell et al. (1995) suggested that the signal could be calculated from the variability between ensemble means (intraensemble variance), and the noise from the variability between individual members around the ensemble mean (interensemble variance). The idea behind this concept is that the ensemble mean is ideally zero unless it is perturbed by external forcing and that the spread of individual members around the ensemble mean is an estimate for the internal variability independent of boundary forcing. We followed this approach and estimated the internal variability by

$$\sigma^2_{\text{int}} = \frac{1}{Y(R-1)} \sum_{y=1}^{Y} \sum_{r=1}^{R} (x_{yr} - \overline{x}_y)^2, \qquad \text{(A1)}$$

where x_{yr} is the quantity under consideration for year y and member r, Y is the total number of years, and R is the total number of members. The overbar denotes ensemble averaging. An estimate of the variability of the ensemble means is given by

$$\sigma^2_{EM} = \frac{1}{Y-1} \sum_{y=1}^{Y} (\overline{x}_y - \overline{\overline{x}})^2, \qquad \text{(A2)}$$

where the double bar denotes climatological ensemble mean. Because of the limited number of members that were used to compute the ensemble mean, the ensemble mean variance still contained some internal variability and thus overestimated the SST-forced variance. An unbiased estimate of the external variability is given by

$$\sigma_{ext}^2 = \sigma_{EM}^2 - \frac{1}{R}\sigma_{int}^2. \quad (A3)$$

Finally, we take

$$\sigma_{total}^2 = \sigma_{ext}^2 - \sigma_{int}^2 \quad (A4)$$

to estimate the total variance of variable x. In the case of observational data, only one member is available, so that only the total variance can be calculated from

$$\sigma^2 = \frac{1}{Y-1}\sum_{y=1}^{Y}(x_y - \bar{\bar{x}})^2. \quad (A5)$$

REFERENCES

Anderson, J., H. Van den Dool, A. Barnston, W. Chen, W. Stern, and J. Ploshay, 1999: Present-day capabilities of numerical and statistical models for atmospheric extratropical seasonal simulation and prediction. *Bull. Amer. Meteor. Soc.,* **80,** 1349–1361.

Boer, G. J., 1995: Analyzed and forecast large-scale tropical divergent flow. *Mon. Wea. Rev.,* **123,** 3539–3553.

Buizza, R., 1997: Potential forecast skill of ensemble prediction and spread and skill distributions of the ECMWF ensemble prediction system. *Mon. Wea. Rev.,* **125,** 99–119.

Chen, S. C., J. O. Roads, and J. C. Alpert, 1993: Variability and predictability in an empirically forced global model. *J. Atmos. Sci.,* **50,** 443–463.

Chen, T. C., and J. C. Alpert, 1990: Systematic errors in the annual and intraseasonal variations of the planetary-scale divergent circulation in NMC medium-range forecasts. *Mon. Wea. Rev.,* **118,** 2607–2623.

Ferranti, L., T. N. Palmer, F. Molteni, and K. Klinker, 1990: Tropical–extratropical interaction associated with the 30–60 day oscillation and its impact on medium and extended range prediction. *J. Atmos. Sci.,* **47,** 2177–2199.

Fink, A., and P. Speth, 1997: Some potential forcing mechanisms of the year-to-year variability of the tropical convection and its intraseasonal (25–70-day) variability. *Int. J. Climatol.,* **17,** 1513–1534.

Flatau, M., P. J. Flatau, P. Phoebus, and P. P. Niiler, 1997: The feedback between equatorial convection and local radiative and evaporative processes: The implications for intraseasonal oscillations. *J. Atmos. Sci.,* **54,** 2373–2386.

Graham, N. E., and T. P. Barnett, 1987: Sea surface temperature, surface wind divergence and convection over tropical oceans. *Science,* **238,** 657–659.

Gutzler, D. S., 1991: Interannual fluctuations of intraseasonal variance of near-equatorial zonal winds. *J. Geophys. Res.,* **96C,** 3173–3185.

Hayashi, Y., and D. G. Golder, 1993: Tropical 40–50-day and 25–30-day oscillations appearing in realistic and idealized GFDL climate models and the ECMWF dataset. *J. Atmos. Sci.,* **50,** 464–494.

Hendon, H. H., C. D. Zhang, and J. D. Glick, 1999: Interannual variation of the Madden–Julian oscillation during austral summer. *J. Climate,* **12,** 2538–2550.

——, B. Liebmann, M. Newman, J. D. Glick, and J. E. Schemm, 2000: Medium-range forecast errors associated with active episodes of the Madden–Julian oscillation. *Mon. Wea. Rev.,* **128,** 69–86.

Higgins, R. W., and K. C. Mo, 1997: Persistent North Pacific circulation anomalies and the tropical intraseasonal oscillation. *J. Climate,* **10,** 223–244.

Jones, C., D. E. Waliser, J. K. E. Schemm, and W. K. M. Lau, 2000: Prediction skill of the Madden and Julian Oscillation in dynamical extended range forecasts. *Climate Dyn.,* **16,** 273–289.

——, ——, K. M. Lau, and W. Stern, 2004: The Madden–Julian oscillation and its impact on Northern Hemisphere weather predictability. *Mon. Wea. Rev.,* **132,** 1462–1471.

Krishnamurti, T. N., D. K. Oosterhof, and A. V. Mehta, 1988: Air–sea interaction on the time scale of 30 to 50 days. *J. Atmos. Sci.,* **45,** 1304–1322.

Kuma, K., 1994: The Madden and Julian oscillation and tropical disturbances in an aqua-planet version of JMA global model with T63 and T159 resolution. *J. Meteor. Soc. Japan,* **72,** 147–172.

Lau, K. M., and F. C. Chang, 1992: Tropical intraseasonal oscillation and its prediction by the NMC operational model. *J. Climate,* **5,** 1365–1378.

Lorenc, A. C., 1984: The evolution of planetary-scale 200-mb divergent flow during the FGGE year. *Quart. J. Roy. Meteor. Soc.,* **110,** 427–441.

Madden, R. A., and P. R. Julian, 1994: Observations of the 40–50-day tropical oscillation—A review. *Mon. Wea. Rev.,* **122,** 814–837.

Maloney, E. D., and J. T. Kiehl, 2002: MJO-related SST variations over the tropical eastern Pacific during Northern Hemisphere summer. *J. Climate,* **15,** 675–689.

Moorthi, S., and M. J. Suarez, 1992: Relaxed Arakawa–Schubert: A parameterization of moist convection for general circulation models. *Mon. Wea. Rev.,* **120,** 978–1002.

Reichler, T., and J. O. Roads, 2005: Long-range predictability in the Tropics. Part I: Monthly averages. *J. Climate,* **18,** 619–633.

Rowell, D. P., C. K. Folland, K. Maskell, and M. N. Ward, 1995: Variability of summer rainfall over tropical North Africa (1906–92)—Observations and modelling. *Quart. J. Roy. Meteor. Soc.,* **121,** 669–704.

Schemm, J. E., H. Van den Dool, and S. Saha, 1996: A multi-year DERF experiment at NCEP. Preprints, *11th Conf. on Numerical Weather Prediction*, Norfolk, VA, Amer. Meteor. Soc., 47–49.

Schubert, S. D., and M. L. Wu, 2001: Predictability of the 1997 and 1998 south Asian summer monsoon low-level winds. *J. Climate,* **14,** 3173–3191.

Slingo, J. M., and R. A. Madden, 1991: Characteristics of the tropical intraseasonal oscillation in the NCAR Community Climate Model. *Quart. J. Roy. Meteor. Soc.,* **117,** 1129–1169.

——, and Coauthors, 1996: Intraseasonal oscillations in 15 atmospheric general circulation models—Results from an AMIP diagnostic subproject. *Climate Dyn.,* **12,** 325–357.

——, D. P. Rowell, K. R. Sperber, and E. Nortley, 1999: On the predictability of the interannual behaviour of the Madden–Julian Oscillation and its relationship with El Niño. *Quart. J. Roy. Meteor. Soc.,* **125,** 583–609.

Toth, Z., and E. Kalnay, 1993: Ensemble forecasting at NMC: The generation of perturbations. *Bull. Amer. Meteor. Soc.,* **74,** 2317–2330.

——, and ——, 1997: Ensemble forecasting at NCEP and the breeding method. *Mon. Wea. Rev.,* **125,** 3297–3319.

Van den Dool, H. M., and S. Saha, 1990: Frequency dependence in forecast skill. *Mon. Wea. Rev.,* **118,** 128–137.

Waliser, D. E., C. Jones, J. K. E. Schemm, and N. E. Graham, 1999a: A statistical extended-range tropical forecast model based on the slow evolution of the Madden–Julian oscillation. *J. Climate,* **12,** 1918–1939.

——, K. M. Lau, and J. H. Kim, 1999b: The influence of coupled sea surface temperatures on the Madden–Julian oscillation: A model perturbation experiment. *J. Atmos. Sci.,* **56,** 333–358.

——, ——, W. Stern, and C. Jones, 2003: Potential predictability of the Madden–Julian oscillation. *Bull. Amer. Meteor. Soc.,* **84,** 33–50.

Weller, R. A., and S. P. Anderson, 1996: Surface meteorology and air–sea fluxes in the western equatorial Pacific warm pool during the TOGA coupled ocean–atmosphere response experiment. *J. Climate,* **9,** 1959–1990.

Winkler, C. R., M. Newman, and P. D. Sardeshmukh, 2001: A linear model of wintertime low-frequency variability. Part I: Formulation and forecast skill. *J. Climate,* **14,** 4474–4494.

Wu, M. L. C., A. Schubert, I. S. Kang, and D. Waliser, 2002: Forced and free intraseasonal variability over the South Asian monsoon region simulated by 10 AGCMs. *J. Climate,* **15,** 2862–2880.

Zhang, C., 1996: Atmospheric intraseasonal variability at the surface in the tropical western Pacific Ocean. *J. Atmos. Sci.,* **53,** 739–758.